International Journal of Methodology

Volume 4, Issue 1, pp. 1-15, 2026
DOI: https://doi.org/10.21467/ijm.4.1.9492

Automatic Calculation of the Rheoencephalographic Pulse Wave Peaks: The First Results

Istvan Pinter[1], Mihaly Bagany[1], Sandor Szabo[2, 3], Michael Bodo[4*]

[1] John von Neumann University, Kecskemet, Hungary
[2] University of Szeged, Faculty of General Medicine, Department of Aviation and Space Medicine, Kecskemét, Hungary
[3] Hungarian Defence Forces Medical Center, Aeromedical, Military Medical Screening and Healthcare Institute, Kecskemét, Hungary
[4] Uniformed Services University of the Health Sciences, Bethesda, MD, USA

Corresponding author's e-mail: michaelbodo1947@gmail.com
Received: 30 August 2024 / Revised: 19 May 2025 / Accepted: 18 January 2026 / Published: 27 January 2026

ABSTRACT

To create an algorithm to detect rheoencephalographic (REG) pulse wave second peak increase, which may detect an increase in intracranial pressure (ICP). REG was measured in 19 healthy volunteers during control and a 15-degree head-down tilt (HDT), which caused an increase in ICP. We developed an algorithm for automatically calculating P1 and P2 from the REG pulse waveform. The result was compared to manual measurements during control and HDT positions. The automatic determination of the peaks' time instants was considered a series of two-class decision problems in ±15-ms-wide sliding decision windows. We achieved an accuracy of 0.9826, a sensitivity of 0.7727, and a specificity of 0.9902. We used the correlation coefficient between manual measurements and automated data and the normalized mean absolute error (NMAE) metric to characterize the precision of peak amplitude value estimation. We achieved a high correlation (> 0.8) in 92% of all tests, and NMAE < 0.3 in 96%. The remaining cases were analyzed using Bland-Altman plots to uncover the main causes of differences. We tested the hypothesis of increasing P2 peak amplitude during HDT compared to the control position. In the female group, the number of significant increases was 4 out of 6 (67%), both in manual and automatic measurements. In the case of the male group's manual measurements, 12 of 13 (92%), and the automatic calculation gave 10 of 13 (77%). The significance is to switch from invasive ICP to noninvasive REG to have the same information for decision-making at the bedside to save the lives of neurocritical care patients. Future REG correlation studies suggested using REG in neurocritical care monitoring, space research, and military medical practice.

Keywords: Pulse wave morphology, Rheoencephalogram, Noninvasive

1 Introduction

1.1 Intracranial Pressure

The goal of neuromonitoring is to prevent secondary brain damage. Invasive ICP monitoring is the gold standard in neurocritical care. It is documented in publications and society consensus statements [1-6]. Later, it was noted that "ICP is more than a number" [7], referring to the information that the pulse wave morphology change can represent. The ICP pulse waveform usually exhibits three distinct local maxima, or peaks, denoted as peak 1 (P1 - percussion wave), P2 (tidal wave), and P3 (dicrotic wave), with P2 and P3 separated by the dicrotic notch. Analysis of ICP pulse waves is a new method for determining intracerebral compliance [8]. The characteristic change in the ICP pulse wave morphology during decreased intracranial compliance is the elevation of P2 [9]. The comprehensive clinical aspect of ICP elevation was published [10,11]. The consequence of computerized monitoring has resulted in several new methods, specifically the analysis of ICP pulse waves [12-19]. Measuring the P2/P1 ratio is used in the B4C system, a noninvasive

intracranial compliance monitoring device [17, 20]. The P1/P2 ratio of the ICP pulse wave was analyzed [19]. Since the ICP elevation is not the only source of brain damage, other modalities are also suggested to monitor cerebral blood flow (CBF) and its autoregulation (AR). The status of CBF AR – cerebrovascular reactivity - is tested with CO_2 inhalation, breath-holding, and acetazolamide (Diamox) infusion. For continuous monitoring of CBF AR, a program was developed, called ICM+ [21]. It calculates the pressure reactivity index (PRx) from *invasive* ICP and arterial pressure pulse waves.

1.2 Rheoencephalography

Rheoencephalography (REG) is a bioimpedance measuring method. REG is acknowledged by the United States of America Food and Drug Administration to measure cerebral circulation [22]. The physical basis of the REG pulse wave is that the brain has a higher electrical resistivity than the blood and cerebrospinal fluid [23]. During the heart ventricular contraction, the blood, i.e., a volume of better conductor, is pumped into the cranial cavity, causing decreased electrical resistance. Early studies described that it is good to indicate an increase in ICP [23,24]. An *in vitro* study demonstrated that a bioimpedance pulse wave amplitude is proportional to the fluid (0.9 % NaCl) volume change [25]. Human measurement showed that cerebral blood volume (measured by isotope) increased during CO_2 inhalation, and it is reflected identically in ICP and processed REG amplitude increase [26]. An *animal study* documented that REG reflects an identical rise in ICP during vinpocetine injection; the area under the curve was 0.95 for REG time constant 3 and 0.93 for REG time constant 0.3; both with $p<0.0001$ [27]. When the CBF AR index is calculated from bioimpedance pulse waves (REG and arm pulse waves), it is called REGx. A human study documented that the CBF AR index measured by REG (REGx) and REG pulse wave morphology change (P2) coincided: when CBF AR was passive, the REG P2 peak was higher, and when CBF AR was active, REG P1 was higher [28]. Details of the REG pulse wave influencing factors can be found here [29]. Several REG correlation/validation studies were summarized here [30,31].

1.3 Head-down Tilt Test

The Trendelenburg or head-down tilt (HDT) position is used in clinical practice and research (as ground-based simulated weightlessness settings). The damped venous outflow during HDT causes an increase in ICP. We hypothesized that the REG pulse wave morphology would change (P2>P1) during the HDT position. The result of the manual calculation of REG P2 and REGx was published previously [32]. Here we present the method and the result of the automated analysis and its comparison to the manual analysis.

2 Materials and Methods

The study was conducted in the Aeromedical, Military Screening, and Healthcare Institute, Medical Centre, Hungarian Defense Forces, Kecskemet, Hungary. The test procedure was conducted by the Declaration of Helsinki and was approved by the Medical Research Ethics Review Board of the Ministry of Defense, Budapest, Hungary, on September 16, 2020. Each subject provided written informed consent before participating. After obtaining information about the purpose and details of the tests, the subjects signed the consent form. No external funding was received.

2.1 Study Population

We measured 19 healthy volunteers (6 females and 13 males). They were two- to four-year pilot cadets. They were in a horizontal, supine position on the tilting table during the measurement. The length of the recordings was 45.47 ± 5.45 (mean ± SD) minutes. The challenge was the HDT (– 15-degree) position, which lasted for 17.62 (±2.39) minutes. Another test was a 30-second breath-holding test, the results of which were reported separately [32].

The mean age (n=19) was 22.68 ± 1.49 years, the mean height was 177.63 ± 6.18 cm, and the mean body mass index (BMI) was 22.94 ± 2.43. There was no significant difference in BMI between the male and female groups. There was a significant group difference in weight (males 76.62 ± 7.16 kg and females

63.33 ±3.98 kg; p=0.0001). Abdominal circumference was also significantly different (p=0.03): males (84.31 ± 5.41 cm) and females (75.17 ± 7.81 cm).

2.2 Data Acquisition

Electrodes were placed while volunteers were in a sitting position. Before electrode placement, the skin was cleaned with benzine and EEG cleaning paste. The electrodes were regular electrocardiogram (EKG) electrodes. Their location was bifrontal: Fp1-Fp2 according to the electroencephalogram (EEG) 10-20 International System of Electrode Placement [33]. A bipolar bioimpedance amplifier (ReoRON-61, Medicor, Esztergom, Hungary) was used with an additional amplifier (BK-094-1; Elsoft BT, Budapest, Hungary) to amplify, filter, and switch signals from symmetrical to asymmetrical. For analog-digital conversion, a 16-bit resolution device was used (NI USB-6211, National Instruments, Austin, TX). Data collection was performed with a laptop (Alienware, Dell, Round Rock, TX) and DataLyser (DL) [34] software. The sampling rate was 200 Hz. Event markers were stored on a separate channel, together with the bioimpedance pulse waveforms. DL creates deidentified files by automatically generating both waveform (binary) and meta files (ASCII) with manually entered notes.

2.3 Data Analysis

We elaborated a novel P1 and P2 detection algorithm for REG signals. An ideal algorithm should have the following properties: 1) it detects and handles missing data during the measurement process, 2) it locates artifacts and extracts the REG-pulse wave from the noisy signal, 3) it determines the (time instant, peak amplitude) value-pairs of P1, P2 peaks, 4) it can adaptively adjust parameters to patient's physiological quantity during measurement. Our recent algorithm deals with the 3rd and 4th problems when the REG-signal part, containing the P1 and P2 peaks, is known in advance. The locations in peaks are about the maximum value of the REG-pulse wave. The P1 and P2 candidates are local maximum and inflection points in this neighborhood. Therefore, the rule-based algorithm decides which is to be marked as P1 and P2 from candidate points and operates in the time domain. We elaborated the rules experimentally during the algorithm development process using manually measured peaks and all measured REG signals in the tilting table tests. The overall duration of REG signals involved was 13820 seconds for the female group and 36795 seconds for the male group (a total of approximately 14 hours). We realized and tested the algorithm in the MATLAB environment [35].

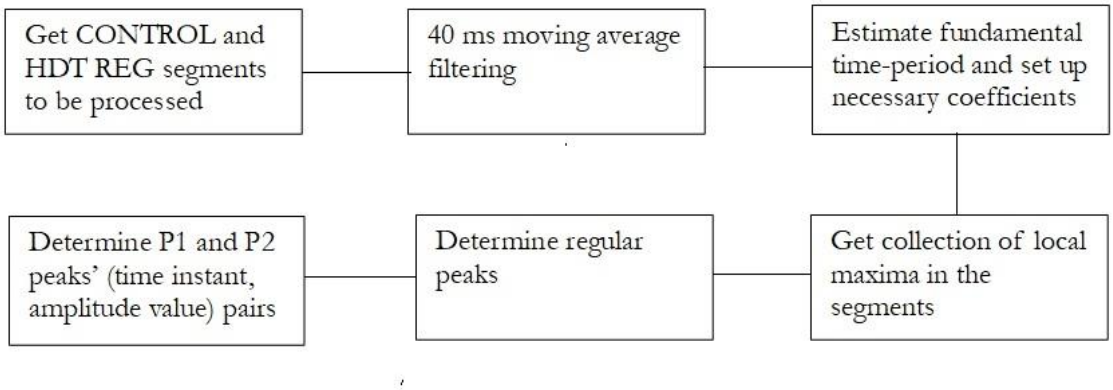

Figure 1: *A flowchart or simplified schematic, and the processing pipeline.*

Because of the rich morphology of REG-pulse waves, we introduced the concepts of *regular peaks* and the *neighborhood of the actual regular peak*, where P1 and P2 should occur. The neighborhood consists of two time slots around the actual regular peak: one is before, and the other is after the peak. Concerning the concept of regular peaks, we found that in several cases, there are spurious local maxima in the signal segment in question, which are not allowed in the estimation of P1 and P2 peaks. Regular peaks are those involved in the determination of (time instant, amplitude value) pairs of the peaks. Moreover, in the right

time slot, we determine not only the closest local maximum but the inflection point, too. The computation of the latter is important, because in several cases the P2 is not a local maximum, but an inflection point in this timeslot. With these concepts, the processing pipeline consists of six main steps, illustrated in Figure 1.

2.4 Detailed Description of the Algorithm

In the following, the explanations of each step will be given.

1. *Extraction of REG-signal parts from the measured signal, both in the control and HDT tests*
   This step is based on manually measured P1s' and P2s' time values. The first- and last-time value of the corresponding ascending sorted list is the basis of the extraction.
2. *Suppressing the contaminating 50 Hz noise and its harmonics*
   We used two-pass 40-ms moving average filtering for this purpose. This linear phase digital filter acceptably suppresses the noise while preserving the REG-signal morphology.
3. *Computation of the fundamental time-period of the REG-signal part to ensure patient-adaptivity*
   The amplitude spectrum of the signal part is estimated with a Hamming window, and the F_{REG} the frequency of maximum amplitude is determined in the $[0.67; 2.33]$ Hz band. The fundamental time period is the reciprocal value of that frequency: $T_{REG} = 1/F_{REG}$.
4. *Determining the collection of local maxima in the REG-signal part*
   We used for this purpose the algorithm, published in [36]. The main advantage of this method, that no experimental threshold values are needed when determining the local maximum. Thus, the number of parameters of the whole P1 and P2 estimation process can be decreased substantially. This algorithm (with a little modification) was used for ICP signal processing in [37].
5. *Determining regular peaks from the collection of local maxima*
   We determined regular peaks in two consecutive steps:
   5.1. For each local maximum, we exclude those for which the inequality below does not hold: $REG_{avg} - 3 \cdot REG_{sd} \leq REG^{peak}_{regular\ peak\ candidate} \leq REG_{avg} + 3 \cdot REG_{sd}$, where REG_{avg} is the average REG_{sd} is the standard deviation of local maxima in the collection,
   5.2. From the remaining regular peak candidates, we also exclude those where $\Delta T_{i,i+1}$the time difference between two consecutive such peaks is too short: $\Delta T_{i,i+1} < 0.5 \cdot T_{REG}$.
6. *Determination of P1 and P2 peaks' (time instant, amplitude value) data pairs*
   First, we determined with numerical experiments the neighborhood of the $P(t_{actual}, REG_{actual})$ actual regular peak, where P1 and P2 should occur. The width of the timeslot is given as a time interval of $[0{,}05 \cdot T_{REG}; 0{,}5 \cdot T_{REG}]$. In the left timeslot, we determined that local maximum, $(t^{max}_{left}, REG^{max}_{left})$, which is closest to the actual regular peak. In the right time slot, we determine not only the closest local maximum, $(t^{max}_{right}, REG^{max}_{right})$, but the inflection point, $(t^{infl}_{right}, REG^{infl}_{right})$, too. With these four points, we determine the peaks with the decision rules below:

   IF $REG^{max}_{left} > REG^{max}_{right}$ AND $REG^{max}_{left} > 0.75 \cdot REG_{actual}$ THEN

   $$P_1 = (t^{max}_{left}, REG^{max}_{left}) \quad P_2 = P(t_{actual}, REG_{actual}),$$

   ELSE IF $REG^{infl}_{right} > REG^{max}_{right}$ THEN

   $$P_1 = P(t_{actual}, REG_{actual}) \quad P_2 = (t^{infl}_{right}, REG^{infl}_{right})$$

   ELSE

   $$P_1 = P(t_{actual}, REG_{actual}) \quad P_2 = (t^{max}_{right}, REG^{max}_{right})$$

Figures 2 and 3 illustrate the P1 and P2 detection results graphically, both in control and HDT positions.

DOI: 10.2147/ijm
Available online at Journals.aijr.org

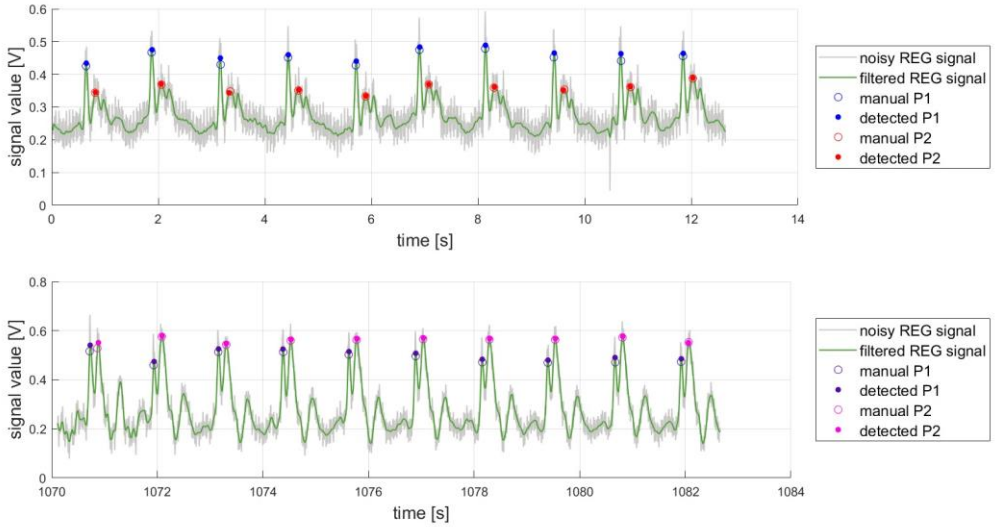

Figure 2: *Manual and automatic P1, P2, and the REG signal – first in a series of 19 measurements (upper trace: control, lower trace: HDT position).*

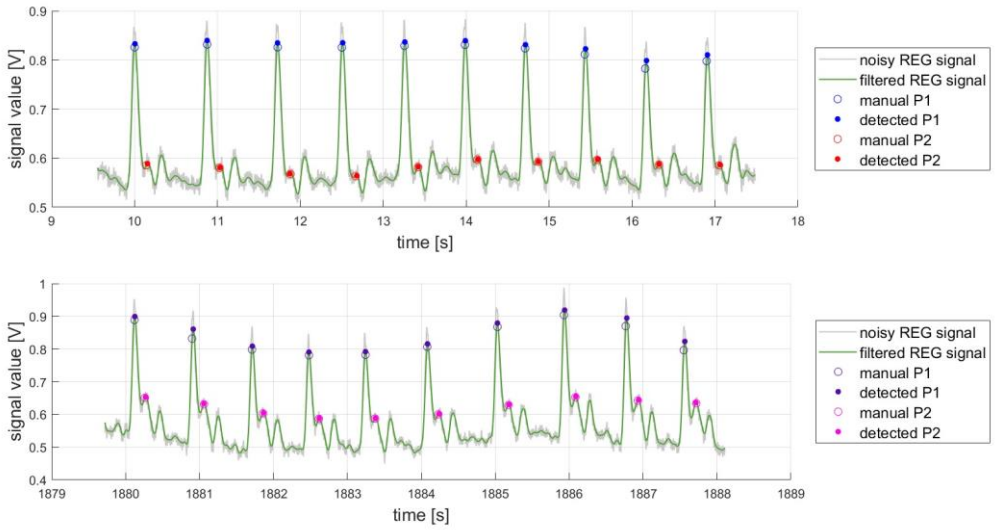

Figure 3: *Manual and automatic P1, P2, and the REG signal – last in a series of 19 measurements (upper trace: control, lower trace: HDT position).*

3 Results

3.1 The Evaluation of the Algorithm

We wrote a MATLAB program for the evaluation of the realized algorithm. We have two collections (manual, and automatic) of P1s, and P2s both in control and HDT to evaluate. There are two parameters of the algorithm to evaluate: 1) the precision of the time value created by the automatic procedure, and 2) the precision of the amplitude value estimation. Both can be evaluated because of the availability of the corresponding manual measurements.

We considered the *first problem* as a *two-class decision problem* on the "grid" of evenly spaced sampling time instants. We characterized the decision with the detection window of a given length and determined the optimal detection window length using the ROC (Receiver Operating Characteristics) analysis [38]. We moved this detection window alongside the REG-signal part, which results in a series of detection windows and a series of decisions. In the actual detection window, it can be decided whether the manually measured

DOI: 10.2147/ijm
Available online at Journals.aijr.org

time value is present or not, as is the case with the automatically determined time value. Therefore, for a given detection window length, the confusion matrix can be determined. From the confusion matrix, the (false positive rate, true positive rate) data pair can be computed, which is a point of the empirical ROC curve. Repeating this process for several detection time-windows, not only can the points of the empirical ROC be determined, but the AUC (Area Under the Curve) can also be estimated: $0 \leq AUC \leq 1$, ideally 1. We achieved AUC = 0.9196 concerning all control and HDT test signal sections. For a final decision time window, however, we haven't selected the optimal one (corresponding to the closest point of the ROC-curve to P (0;1) point), because it was ±25 ms wide; we used instead a narrower one (±15 ms) as a suboptimal solution for remaining computations. With this decision time window, we achieved acceptable values of sensitivity (0.7727), specificity (0.9902), and F1-score (> 75%). Concerning the *second problem*, the precision of amplitude value estimation, it is important to note that during the evaluation of time value estimation described above, the matching data pairs of manual and automatic measurements can also be collected, which is necessary for the evaluation of amplitude value estimation.

For numerical characterization of precision, we used both the *correlation coefficient and NMAE* (Normalized Mean Absolute Error): $NMAE = \frac{\frac{1}{N}\sum_{i=1}^{N}\left|y_i^{manual} - y_i^{automatic}\right|}{y_{max}^{manual} - y_{min}^{manual}}$, where N is the number of corresponding data pairs, y_i^{manual} is the manually measured, $y_i^{automatic}$ is the value determined automatically, and $y_{max}^{manual} - y_{min}^{manual}$ is the range of manually measured values. We selected the normalized MAE because the dynamic ranges of different REG-signal parts are very distinct, and NMAE is invariant to multiplication with a constant. Therefore, this property makes it possible to compare the precision results of different REG-signals. We achieved a high correlation (> 0.8) in 92% of all tests, and NMAE < 0.3 in 96%. The remaining cases were analyzed using Bland-Altman plots [39] for uncovering the main causes of differences. Typical plots can be seen in Figure 4. By carefully examining the corresponding REG-signal part, it can be concluded that by repeating the manual measurements, the one outlier point is expected to disappear.

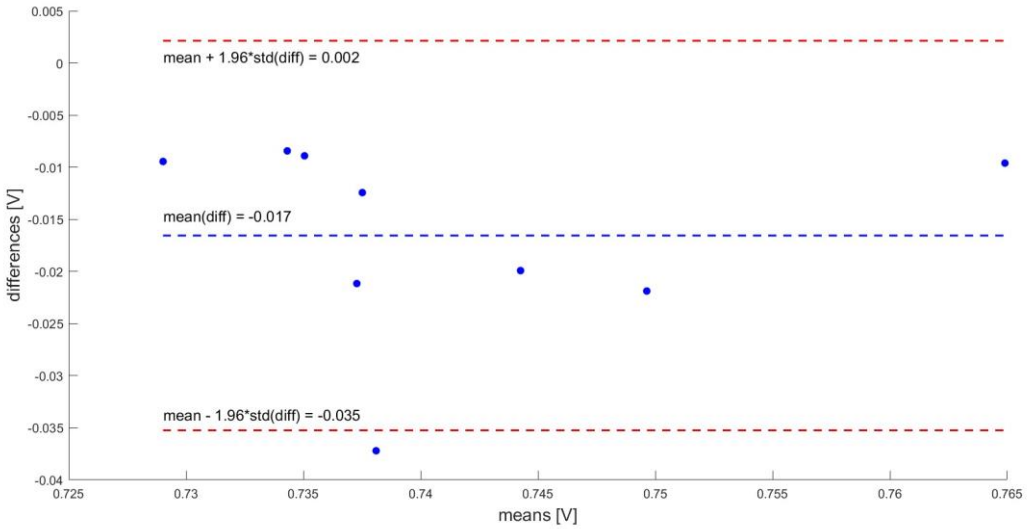

DOI: 10.2147/ijm
Available online at Journals.aijr.org

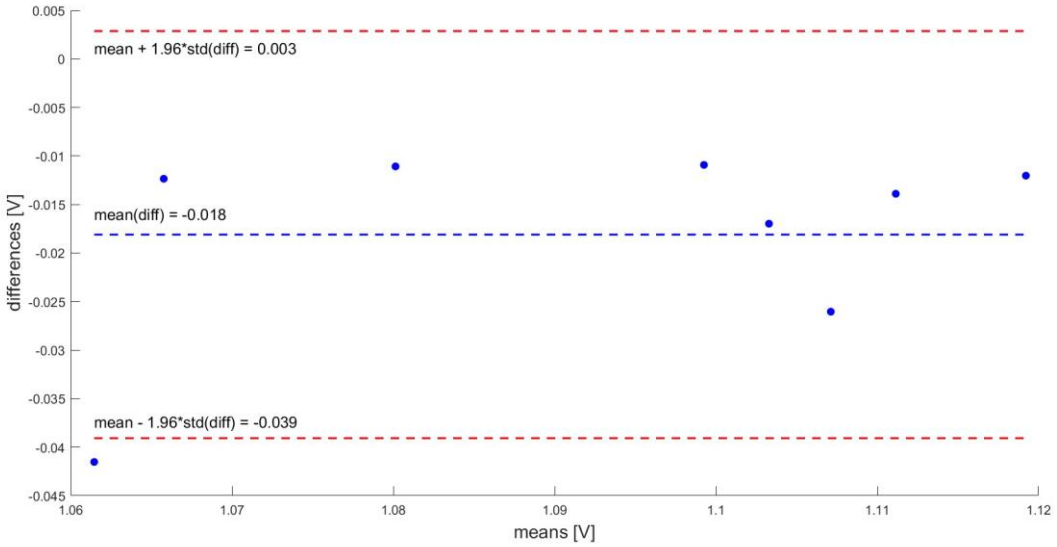

Figure 4: *Typical Bland-Altman plots with one outlier point (blue point below the lower dashed red line; upper trace: male, lower trace: female)*

3.2 Statistical Tests for Increasing P2 During HDT, Comparison of Manual and Automatic Data

We wrote a MATLAB program to test the hypothesis of increasing P2 amplitude during HDT compared to the control position. To accept or reject the assumption of increasing P2 during HDT, we first checked the normality using the Lilliefors test. If the null hypothesis for normality passed, the paired t-test was applied to test the equality of means. If the normality hypothesis was rejected, we used the Wilcoxon rank sum test for equal medians. The male and female groups were tested separately; the significance level in both cases was $p < 0.05$. In the female group, the number of significant increases was 4 out of 6 (67%), both in manual and automatic measurements. The detailed results are in Table 1.

Table 1: *Comparative result of paired t-test in case of a female group (ID: identifier of REG measurement; P2 control and HDT values are sample means in volt [V]).*

ID	Manually measured values					Automatically determined values				
	P2 control	P2 HDT	signifi-cant?	p	Cohen's d	P2 control	P2 HDT	signifi-cant?	p	Cohen's d
06_1	0.6528	0.648	no	0.787	0.1509	0.637	0.6497	no	0.49	-0.4007
11_1	0.5986	0.6384	*yes*	< 0.001	-2.4895	0.5997	0.6403	*yes*	< 0.001	-2.41
14_1	0.4601	0.4823	*yes*	< 0.001	-1.9273	0.4617	0.4854	*yes*	< 0.001	-2.2159
19_1	0.5898	0.6615	*yes*	< 0.001	-3.2987	0.594	0.6626	*yes*	< 0.001	-3.1299
25_1	0.5813	0.593	no	0.353	-0.3787	0.597	0.6095	no	0.464	-0.2767
25_2	0.8709	1.0454	*yes*	< 0.001	-6.8787	0.8747	1.049	*yes*	< 0.001	-6.9055

In the case of the male group's manual measurements, 12 out of 13 (92%) showed significant increases, while the automatic calculation yielded 10 out of 13 (77%). The detailed results of t-tests can be seen in Table 2, and those of Wilcoxon tests in Table 3.

DOI: 10.2147/ijm
Available online at Journals.aijr.org

Table 2: *Comparative result of paired t-test in case of a male group (ID: identifier of REG measurement; P2 control and HDT values are sample means in volts [V]).*

ID	Manually measured values					Automatically determined values				
	P2 control	P2 HDT	signifi-cant?	p	Cohen's d	P2 control	P2 HDT	signifi-cant?	p	Cohen's d
05_1	0.3575	0.5586	*yes*	< 0.001	-13.139	0.3579	0.564	*yes*	< 0.001	-14.426
05_2	0.306	0.3684	*yes*	0.004	-2.2411	0.285	0.3706	*yes*	< 0.001	-2.3335
06_2	0.3427	0.3528	no	0.416	-0.4203	0.3446	0.3555	no	0.381	-0.4546
08_1	0.3033	0.3382	*yes*	< 0.001	-2.8177	0.3064	0.3408	*yes*	< 0.001	-2.8344
12_1	0.5825	0.6269	*yes*	< 0.001	-2.1123	0.5826	0.6276	*yes*	< 0.001	-2.1641
19_2	0.6066	0.6421	*yes*	< 0.001	-1.2504	0.617	0.6445	*yes*	0.006	-0.9304
20_1	0.5873	0.7128	*yes*	< 0.001	-7.7243	see Table 3				
21_1	0.6523	0.7484	*yes*	< 0.001	-4.1359	see Table 3				
21_2	0.8565	0.9734	*yes*	< 0.001	-2.9291	0.8589	0.9776	*yes*	< 0.001	-3.0029
22_1	0.5584	0.6275	*yes*	0.002	-1.5375	see Table 3				
26_1	0.9094	0.9463	*yes*	0.026	-0.9899	0.917	0.9463	no	0.062	-1.0339
26_2	0.5837	0.6219	*yes*	< 0.001	-1.8773	0.5848	0.6235	*yes*	< 0.001	-1.8824

Table 3: *Comparative result of Wilcoxon -test in case of a male group (ID: identifier of REG measurement; P2 control and HDT values are sample medians in volt [V]).*

ID	Manually measured values					Automatically determined values				
	P2 control	P2 HDT	signifi-cant?	p	median effect size	P2 control	P2 HDT	signifi-cant?	p	median effect size
20_1	see Table 2					0.5897	0.7199	*yes*	< 0.001	-0.1302
20_2	0.4356	0.4474	*yes*	0.017	-0.0118	0.4429	0.4489	*yes*	0.005	-0.006
21_1	see Table 2					0.6526	0.7542	*yes*	< 0.001	-0.1016
22_1	see Table 2					0.5616	0.607	no	0.064	-0.0454

The statistical results of manual data were better than those of automatic. However, it is also clear that a refined definition of P2 peaks in the case of REG pulses could also be important; first of all, the transition of P2 from inflection point to local maximum.

4 Discussion

In this descriptive study, we describe the first time the results, what we got using a MATLAB script for automatic peak calculation of the REG pulse wave and comparing these results to those that we got by using manual cursor operation, which was published previously [32]. In other publications, we used a DataLyser program [34]. The P2 increase in REG pulse waves during HDT is a novelty. Such a change was typically described previously on invasive ICP waveform morphology. Computerized noninvasive ICP monitoring was reported by [40]. In recent years, a few ICP pulse wave analysis publications have appeared, involving a patent [41], a device [17], a calculation of the P2/P1 ratio [18], and a device for measuring the head's dielectric properties (Cephalotec, Horgen, Switzerland), which is changing as a heartbeat-related pulse wave [42].

Respiration causes a subharmonic in the REG pulse wave and influences the morphology of P2 [48]. We measured and averaged 10 pulse waves to eliminate the effect of inhalation and exhalation with manual measurements. NB: In clinical practice, the CBF measurement with Doppler ultrasound uses only one pulse wave in the report as the result of the CBF measurement.

There are discrepancies between manual and automatic methods. The explanation is that manual calculation was selected by visual inspection of the pulse waves, i.e., artifacts were excluded. The automated calculation was running without such a selection.

4.1 MATLAB Script

We considered the *first problem* as a series of *two-class decision problems* in evenly spaced, nonoverlapping time intervals (detection windows). The duration of the window was determined using ROC (Receiver Operating Characteristics) analysis [38]. In the actual detection window, four events can occur: A) a manually measured peak can be found, B) a manually measured peak can not be found, C) a detected peak can be found, D) a detected peak can not be found. Therefore, the confusion matrix can be determined by counting the following event pairs: (A, C) → TP (true positive), (A, D) → FN (false negative), (B, C) → FP (false positive), finally event pair (B, D) → TN (true negative). From the confusion matrix, the (false positive rate; true positive rate) data pair can be computed, which is a point of the empirical ROC curve. Repeating this process for all detection window the AUC (Area Under the Curve) can also be estimated. With a ±15 ms window, we achieved an AUC of 0.9195, accuracy of 0.9826, sensitivity of 0.7727, specificity of 0.9902, and F1-score of 0.7565. In this case, the sensitivity of the automated algorithm is significantly lower than the specificity. To our opinion, the potential reasons for this discrepancy are twofold: the decision problem itself and the inevitable presence of artifacts. Concerning the artifacts, by careful investigation of automatically detected P1 and P2 peaks, we concluded, that artifacts caused both FN and FP decisions. Concerning the specificity with the definition of TN/(FP+TN), it can be easily seen that if FP is much lower than TN, the value of specificity will be close to 1. We found, that the proposed automatic detector very rarely detects false-positive peaks, so FP (202) is much more lower than FN (20436), which results in a specificity of 0.9902. In case of sensitivity, with definition of TP/(TP+FN), the situation is different, because the number of ideal TP decisions equals to number of manually measured peaks (about 10), and the number of automatically detected false negative peaks could be comparable with the number of true positive ones. The false negative decision means that there is a manually measured peak in the decision time window, but the automatically detected one is missing. By careful investigation of these situations, we concluded that the automatically determined peak-time values were close to the manually measured ones; therefore, by increasing the duration of the decision time window, the sensitivity could be increased. We repeted the computations with a ±25 ms long window, and thus we achieved the following performance parameters: AUC of 0.9196, accuracy 0.9812, sensitivity 0.8503, specificity 0.9888, and F1-score 0.8325 concerning all control and HDT test signal sections. However, in the following analysis, reported in this paper, we used the more rigorous detector with a decision window of ±15 ms.

Excluding the artifacts during P1 and P2 peak estimation is a very difficult problem, and the complex morphology of both REG pulses and artifacts calls for using machine learning methods when developing an artifact detector. The manual creation of the necessary training dataset, consisting of labelled REG pulses, is our planned further work. The pulses will be characterized with all the samples between beginning and ending time instants, P1 time/value pairs, P2 time/value pairs, and the 'REG pulse' or 'artifact' labels. This also makes it possible to develop a suitable feature extraction algorithm for the classifier. For example, it can be ensured that the number of samples (and thus the dimension of the vectors in the training dataset) will be the same by resampling them appropriately. This also makes it possible to examine the possibility of dimensionality reduction using the autoencoder neural network. For the classifier, our first candidate is the support vector machine with a Gaussian kernel, the second one is a deep neural network. To our opinion, by decreasing the number of false decisions mentioned above, better performance in P1 and P2 detection could be expected.

There are discrepancies between manual and automatic methods. The explanation is that manual calculation was selected by visual inspection of the pulse waves, i.e., artifacts were excluded. The automated calculation was running without such a selection. The CBF reactivity was better for REG than ICP and other modalities in a pig study [53].

4.2 REG

The test of cerebrovascular reactivity is based on the comparison of the control/baseline REG peaks (before the challenge) and during or after the challenge and expressing the result in the percentage of the baseline. If the exhaled CO_2 measurement is available, the CO_2 concentration difference can be used for normalization since the increased CO_2 is the trigger of the REG amplitude increase**.** In this study the P2 amplitude change was in focus, since P2 amplitude increase during HDT was identical to that what was described in ICP pulse wave morphology change during ICP increase (intracranial compliance decrease).

There was an individual difference in the shape of P2, which caused difficulty in the manual evaluation. Some individual female-male differences in measured variables can be related to gender differences in the respiratory system [48]. The discussion of the REG origin received the latest argument of its intracranial origin [49]. The REG signal involved 50 Hz noise, which was eliminated in the case of manual measurements by using an amplifier and 0.1 sec running averaging in DL. Complications of invasive intracranial multimodal monitoring were detailed previously [50]. ICP pulse wave analysis was compared [51]. We plan to imitate such a study with the modification that we'll compare ICP and REG pulse waves in neurocritical care patients. The noninvasive ICP monitoring with REG can be integrated into clinical workflows by creating a small bioimpedance device with generating REG and arm pulse waves, calculating 1) P2 increase, and 2) CBF AR index (REGx), and initiates alarm when CBF AR turns to be passive, indicating the lower limit of CBF AR. This is the time when staff need to start to increase arterial pressure.

Previous studies documented: 1) The correlation between CBF AR calculated between invasive and noninvasive CBF AR measurements [52]; 2) REG pulse wave morphology changed during elevated ICP and correlated with brain imaging in neurocritical care patients [28]; 3) An identical ICP and REG pulse amplitude increase during CO_2 inhalation in a neurocritical care patient [26]; 4) Higher cerebrovascular reaction during CO_2 inhalation in REG and NIRS than in TCD during 30-second breath-holding [32]; 5) REG and ICP pulse amplitudes increased during vinpocetine bolus injection in a rat study [27]; 6) In vitro study documented identical change of bioimpedance and Doppler flow pulse amplitude [25]; 7) The CBF reactivity was better for REG than ICP than other modalities in a pig study [53]. Since our groups were healthy volunteers, the clinical outcome is not applicable. Clinical use of REG monitoring was presented various studies [23, 24, 26, 28, 31, 52, 59]. The direct comparison with invasive ICP data is presented in various studies [26, 27, 31, and 52]. ICP increase during vinpocetine injection correlated with REG pulse amplitude increase. Area under the receiver operating characteristic curve was 0.9481 for ICP–REG time constants 3 and 0.9335 for ICP–REG time constants 0.3; both with < p 0.0001 [27]. The PRx produced an accurate metric of vascular reactivity in this cohort, with the area under the receiver-operator characteristic curves of 0.91. REGx was moderately correlated to the PRx (Spearman $r = 0.63$, $p < 0.0001$; Bland-Altman bias-0.13). The area under the receiver-operator curve for the REGx was 0.86 [52]. Several REG validation/correlation studies were summarized recently [54]. The regulation of cerebral blood flow in humans, as well as its physiology and clinical implications of autoregulation, have been detailed elsewhere [55]. The CBF reactivity was better for REG than ICP and other modalities in a pig study [53].

4.3 Space Research and Military Medical Aspects

The findings can be generalized to other populations with varying ICP conditions, such as astronauts. The Spaceflight Associated Neuro-ocular Syndrome (SANS) is a major concern for human spaceflight. SANS is a disorder that affects astronauts after long-duration space travel, causing swelling of the optic nerve, chorioretinal folds, flattening of the optic globe, and changes in near vision. As many as 70% of astronauts develop SANS, which poses a significant risk for space missions and specifically for long-duration space missions (i.e., missions to Mars) because it can lead to severe vision changes that could jeopardize the ability to function safely or control a spacecraft. Previous studies have suggested that abnormal ICP may be the underlying cause of SANS. Additionally, the elevated CO_2 concentration causes increased brain blood volume. The actuality is that the NASA-funded *Translational Research Institute for Space Health* (TRISH) seeks proposals to measure ICP during commercial spaceflights, and proposals must include non-invasive ICP

estimation techniques. The release date was March 27, 2025. REG measurement can help identify the ICP and/or cerebrovascular components of SANS, detect accelerated cerebrovascular aging, and quantify the effect of antigravity countermeasures [32]. Military medicine application of REG monitoring could be during the transport of wounded service members with brain/blast injuries, as detailed in [32, 60]. Regular ECG electrodes are used for REG and arm bioimpedance pulse measurement. For space research applications, we tested a reusable electrode that does not require alcohol rubbing (Combat medic antimicrobial silver barrier wound dressing made by Silverlon.com)

4.4 Results of Literature Search

ICP and REG measurements were mentioned in several publications [43-47]. The search in PubMed with keywords rheoencephalogram and intracranial pressure resulted in 7 hits (May 14, 2025). Two of them were ours. There have been no new publications in the last two years. PubMed search with keywords peak detection and REG pulse waves resulted in no hits (5/13/2025). A PubMed search with keywords rheoencephalogram and pulse wave resulted in 2 hits: one was during Tai Chi exercise (amplitude increase was reported) and the other was during HDT and lower body negative pressure. Cerebral resistance index was calculated, and pulse change was not reported in the abstract (text is in Chinese). ICP was not measured. REG was used during space flight in the 1970s, but there was no pulse wave morphology analysis nor CBF AR measurements [62]. REG was validated against invasive ICP in various studies [23, 24, 26, 27, 29, 52, 53].

4.5 Progression of the Idea

This topic is typical in the field of biomedical engineering, since biomedical engineering combines biology (in our case, physiology of CBF and its AR) and engineering (hardware creation – in our case, bioimpedance amplifier) to make technological breakthroughs in medical devices, procedures, and patient care. Today, we can add developing software, too. To develop a new noninvasive brain monitor using bioimpedance, we need to set 1) A physiological background (CBF AR) to be measured; 2) Hardware; 3) Software. Previous studies documented that existing REG devices can measure REG signals, and cerebrovascular reactivity (CBF AR) can be calculated. A miniaturized REG device - a simplified Cerberus amplifier [59] replica - was built and used for sleep research [61]. The DataLyser program [34] was developed to display, store, and data processing of physiological signals. The manual cursor operation was used to measure REG pulse wave amplitudes (minimum and maximum amplitude and time numbers). Cerberus system [59] involved predecessors of the DataLyser software (SW). A MATLAB [35] script was created and incorporated as a menu item to calculate PRx/REGx, identical to the ICM+ program [21]. This manuscript describes the latest SW development: a MATLAB script for automated REG pulse wave peak detection. The next step of the SW development will be the alarm criteria determination from REGx: the detection of the lower limit of CBF AR. Such work will be based on a simultaneous recording of invasive (ICP and ABP) and noninvasive (REG and arm bioimpedance) signals in neurocritical care patients [52].

The clinical use of a medical device (in the USA) is first required by the American Medical Association of Medicine (AMA) to approve its use in clinical practice (so the health insurance company will pay for its use). To initiate such a process requires a study to submit to the AMA and after to the FDA. Today, no manufacturer submitted a request to approve their REG device. But there are few REG devices available, without FDA approval, and used. The practical use of the REG device is to attach it to any critical care monitor and calculate the CBF AR index. REG use makes it possible, with computerization, to calculate CBF AR during a CBF AR test and as a function of time (REGx). None of them requires any standard. The measured pulse wave unit is ohms. It has no physiological relevance. Cardiac output is measured noninvasively with tetrapolar devices, which measure not only the basic impedance but also the pulsatile impedance, which is used to calculate the cardiac output. Basis impedance is typically not measured with the bipolar devices that we use. However, we published the difference in basic impedance in the in vivo rat brain measurement. ICP elevation by balloon inflation and saline infusion caused opposite changes in

basic impedance, since saline injection decreased the impedance while balloon inflation increased it. REG was measured by the Minnesota Impedance Cardiograph. REG's first derivative (dZ/dt) was increased in both cases [30].

4.6 Additional REG Applications

Although no ICP measurement is involved, we must mention other populations where REG monitoring (noninvasive!) can be useful: 1) Cerebrovascular arteriosclerotic alteration is detected by elongated REG anacrotic (rising) portion [23, 30, 31, 59]; 2) Cerebrovascular alteration caused by excessive alcohol consumption [31]; 3) Detection of spreading depolarization (SD). SD is the earliest sign of brain metabolic disturbance and can be measured with DC EEG and Ag/AgCl electrodes placed on the cortex. We documented the coincidence of SD with REG slow oscillations [30]. 4) Transient brain vasospasm caused by Pegylated liposomal doxorubicin (Doxil - an anti-cancer drug) infusion before systemic cardiorespiratory reaction. The clinical importance of this fact is that the reaction was caused by complement activation (cytokine storm), which is the main problem of COVID-19 patients in intensive care [63]. 5) Monitoring polytraumatized patients with hemorrhage, when CBF AR can be lost, about ABP < 50 mmHg. CBF AR monitoring can prevent brain damage [55, 57]. 6) If CBF AR is passive and the patient is ventilated with positive end-expiratory pressure (PEEP), decreased CBF can cause brain damage. In such cases, the use of PEEP is safe if CBF AR is monitored [53].

4.7 Limitations

The presented automatic REG pulse wave morphology analysis has not been used yet in neurocritical care patients. However, several automatic analyses were used for ICP pulse waves [12-20]. Unlike electroencephalography (EEG) and electrocardiography (ECG), REG has no standards. Additionally, REG does not offer brain mapping or direct reflection of a brain artery flow like TCD. REG, like EEG, is sensitive to movements and muscle contraction, for example, eye blinking. Any ICP/REG monitor with a P2 detection program is currently unavailable. The recent automatic P2 detection algorithm does not involve any artifact rejection. The units of REG pulse wave peak are in ohms, and it can't be converted to mmHg, which is used in clinical practice to evaluate the status of a patient. The differences in results for males and females were not analyzed, however, the effect of the menstrual cycle on CBF is known [56]. The small size of the male and female groups has low statistical power to accept the difference as biologically relevant. The sensitivity of the automated algorithm (0.7727) is significantly lower than the specificity (0.9902), which may impact its reliability in clinical applications. To clarify this problem, we plan to compare the REG pulse wave to the ICP pulse wave analysis. Our program is not at that level of readiness, as it was created for ICP pulse wave analysis [57]. The European Space Agency (ESA) supported the construction of a miniaturized REG amplifier, which involves P2 detection as well as REGx calculation. The manufacturer will get related ESA and medical electrical safety certificates. The new device development is not yet at the Technical Readiness Level (TRL) [58] today, as the Cerberus system, which was created for primary stroke/cardiovascular prevention screening, finds the high-risk population for arteriosclerosis, and the US FDA has acknowledged it as a "non-significant-risk device.[59].

5 Conclusions

Here we report the first result of a script developed for automatic REG pulse wave peak detection. The REG pulse wave morphology changed in the HDT position, like the ICP pulse, with increased P2. Such automatic calculation is necessary in neurocritical care units, making it possible to generate an automatic trigger for an alarm indicating ICP elevation. Having REG-based noninvasive monitoring has the potential to create an alarm, indicating the lower limit of CBF AR [52], so the staff can act immediately to prevent secondary brain injury caused by brain ischemia/hypoxia. REG monitoring offers 1) reflecting decreased intracranial compliance (increased ICP) and 2) monitoring of the CBF AR index (REGx), detecting the lower limit of CBF AR [52]. The novelty is that the REG P2 automatic calculation was not published

previously. The implications and recommendations are that REG monitoring can be used in neurocritical care, space research, military aviation, transporting wounded military Service Members, civilian emergency medicine, and mass casualty evacuation. Future REG monitors can be an independent device or a module of bedside monitors, like near-infrared spectroscopy (NIRS) and bispectral index (BIS) monitors. Further studies are required to justify that REG could serve as a proxy for invasive ICP monitoring. Our manuscript facilitates combining a REG amplifier with the calculation described, which can create a noninvasive lifesaving bedside monitor. This will be the major outcome. Its significance is the lifesaving of neurocritical care patients. The manuscript offers the know-how. The result will be a miniaturized bioimpedance (REG) amplifier with SW, calculating 1) the REG pulse wave P2 increase, reflecting the increase of ICP (decreasing intracranial compliance), and 2) CBF AR (REGx). A study was initiated to test the new device in healthy volunteers with cerebrovascular reactivity and create a CBF AR standard (REGx).

6 Declarations

6.1 Acknowledgments

Recognition goes to measured volunteers and technical support (Andrea Kalman–Tothne, Aniko Kerekes-Zambone, Levente Varga, Szilveszter Szabo, Laszlo Moczar); Lajos Zoltai, and Jozsef Voros for creating the REG device; Gyorgy Thuroczy to loan the REG device; Lajos Baranyi, Matt Dennie, Kevin Hooftallen, Frederick Pearce for DataLyser development; Istvan Lepsenyi, Daniel Lowy, Matyas Palik, Pal Dunai, Piroska Szalay, and Szilvia Kora for their help.

6.2 Funding Source

Michael Bodo received support from the Hungarian Academy of Sciences to participate in this work (travel grant).

6.3 Informed Consent Statement

Informed consent was taken from the volunteer before the measurement started.

6.4 Competing Interests

The authors declare no competing interests.

6.5 Publisher's Note

AIJR remains neutral with regard to jurisdictional claims in institutional affiliations.

How to Cite this Article:

I. Pinter, M. Bagany, S. Szabo, and M. Bodo, "Automatic Calculation of the Rheoencephalographic Pulse Wave Peaks: The First Results", *Int. J. Methodol.*, vol. 4, no. 1, pp. 1–15. Jan. 2026. https://doi.org/10.21467/ijm.4.1.9492

References

[1] Hawryluk G.W.J, Citerio G. et al (2022) Intracranial pressure: current perspectives on physiology and monitoring. Intensive Care Med. 48:1471-1481. https://doi.org/10.1007/s00134-022-06786-y

[2] Shim Y, Kim J, Kim HS, Oh J, Lee S, Ha EJ (2023) Intracranial Pressure Monitoring for Acute Brain Injured Patients: When, How, What Should We Monitor. Korean J Neurotrauma. 28;19(2):149-161. https://doi.org/10.13004/kjnt.2023.19.e32

[3] Depreitere B, Meyfroidt G, Güiza F (eds) (2021) Intracranial Pressure and Neuromonitoring XVII. Acta Neurochirurgica Supplement (NEUROCHIRURGICA, volume 131). Springer, https://doi.org/10.1007/978-3-030-59436-7

[4] Chesnut R, Aguilera S, Buki A et al (2020) A management algorithm for adult patients with both brain oxygen and intracranial pressure monitoring: the Seattle International Severe Traumatic Brain Injury Consensus Conference (SIBICC). Intensive Care Med. 46:919-929. https://doi.org/10.1007/s00134-019-05900-x.

[5] Le Roux P, Menon DK, Citerio G et al (2014) The International Multidisciplinary Consensus Conference on Multimodality Monitoring in Neurocritical Care: a list of recommendations and additional conclusions: A statement for healthcare professionals from the Neurocritical Care Society and the European Society of Intensive Care Medicine. Neurocrit Care. 21: S282-96. https://doi.org/10.1007/s12028-014-0077-6. 38

[6] Link C.D, Haese T.M, Frigieri G, Brasil S, Vellosa J.C.R, Welling L. (2023) Intracranial compliance and volumetry in patients with traumatic brain injury. Surg Neurol Int.14:246; 1-6. https://doi.org/10.25259/SNI_314_2023

[7] Czosnyka M, Czosnyka Z. (2020) Origin of intracranial pressure pulse waveform. Acta Neurochir (Wien) 162:1815-1817. https://doi.org/10.1007/s00701-020-04424-4

[8] Germon K. (1988) Interpretation of ICP pulse waves to determine intracerebral compliance J. Neurosci. Nurs. 20 344–51
[9] Ellis T, McNames J, Aboy M (2007) Pulse morphology visualization and analysis with applications in cardiovascular pressure signals. IEEE Trans Biomed Eng 54:1552-9 https://doi.org/10.1109/TBME.2007.892918
[10] Godoy DA, Brasil S, Iaccarino C, Paiva W, Rubiano AM (2023) The intracranial compartmental syndrome: a proposed model for acute brain injury monitoring and management. Crit Care.27:137:1-9. https://doi.org/10.1186/s13054-023-04427-4
[11] Cucciolini, G, Motroni, V. & Czosnyka, M (2023) Intracranial pressure for clinicians: it is not just a number. J Anesth Analg Crit Care 3-31:1-13 https://doi.org/10.1186/s44158-023-00115-5
[12] Kasprowicz M, Asgari S, Bergsneider M, Czosnyka M, Hamilton R, Hu X. (2010) Pattern recognition of overnight intracranial pressure slow waves using morphological features of intracranial pressure pulse. J Neurosci Methods 15:190:310-8. https://doi.org/10.1016/j.jneumeth.2010.05.015
[13] Mataczynski C, Kazimierska A, Uryga A, Burzynska M, Rusiecki A, Kasprowicz M (2022) End-to-End Automatic Morphological Classification of Intracranial Pressure Pulse Waveforms Using Deep Learning. IEEE J Biomed Health Inform. 26:494-504. https://doi.org/10.1109/JBHI.2021.3088629
[14] Pérez-Sánchez J, Carrillo de Gea J.M. et al (2021) Intracranial pressure analysis software: A mapping study and proposal. Comput Methods Programs Biomed. 209:106334. https://doi.org/10.1016/j.cmpb.2021.106334
[15] Uryga A, Ziółkowski A, Kazimierska A. et al (2022) CENTER-TBI High-Resolution ICU (HR ICU) Sub-Study Participants and Investigators; CENTER-TBI High-Resolution Sub-Study Participants and Investigators. Analysis of intracranial pressure pulse waveform in traumatic brain injury patients: a CENTER-TBI study. J Neurosurg. 23;139:201-211. https://doi.org/10.3171/2022.10.JNS221523
[16] Brasil S. (2022) Intracranial pressure pulse morphology: the missing link? Intensive Care Med. 48:1667-1669. https://doi.org/10.1007/s00134-022-06855-2
[17] brain4care (Brain4care Corp., São Carlos, Brazil) https://brain4.care/en/solution/
[18] Brasil S, Frigieri G, Taccone F.S. (2023) Noninvasive intracranial pressure waveforms for estimation of intracranial hypertension and outcome prediction in acute brain-injured patients. J Clin Monit Comput. 37:753-760. https://doi.org/10.1007/s10877-022-00941-y
[19] Kazimierska A, Manet R, Vallet A et al (2023). Analysis of intracranial pressure pulse waveform in studies on cerebrospinal compliance: a narrative review. Physiol Meas. 4410TR01:1-20. https://doi.org/10.1088/1361-6579/ad0020
[20] Brasil S, Solla DJF, Nogueira RC et al, (2021) A Novel Noninvasive Technique for Intracranial Pressure Waveform Monitoring in Critical Care. J Pers Med. 11:1302. https://doi.org/10.3390/jpm11121302
[21] ICM+: Intensive care Monitoring program. https://icmplus.neurosurg.cam.ac.uk/
[22] Anonymous (1997) Rheoencephalograph (a) Identification Code of Federal Regulations Title 21, vol 8, Sec 882.1825, Washington DC: US Government Printing Office; Revised as of April 1, 1997.
[23] Jenkner FL (1986) Clinical rheoencephalography: a noninvasive method for automatic evaluation of cerebral hemodynamics. Ertldruck, A-6000, Vienna
[24] McHenry LC (1965) Rheoencephalography: a clinical appraisal. Neurology 15:507-17. https://doi.org/10.1212/WNL.15.6.507
[25] Bodo M, Garcia A, Pearce F, vanAlbert S, Armonda R (2010) Influence of volume and change on the electrical impedance signal (in vitro). J. Phys.: Conf. Ser. 22 012111 https://doi.org/10.1088/1742-6596/224/1/012111
[26] Bodo M, Racz J, Ilias L, et al (1986) Rheoencephalographic changes during increased intracranial pressure. In: Krieglstein J. (ed) Pharmacology of Cerebral Ischemia. Elsevier, Amsterdam, pages 265-269. LC : 86029027, ISBN : 0444808450, ISBN : 9780444808455
[27] Bodo M, Simovic M, Pearce F, Ahmed A, Armonda R (2015) Correlation of rheoencephalogram and intracranial pressure: results of a rat study. Physiol. Meas. 36; N115-N126. http://dx.doi.org/10.1088/0967-3334/36/10/N115
[28] Cannizzaro L.A., Iwuchukwu I, Rahaman V, Hirzallah M, Bodo M. (2023) Noninvasive neuromonitoring with rheoencephalography: a case report. J Clin Monit Comput. 19:1–10. https://doi.org/10.1007/s10877-023-00985-8
[29] Moskalenko Y.E. (ed) (1980) Biophysical Aspects of Cerebral Circulation. Pergamon, Oxford, ISBN 0-08-022672-8
[30] Bodo M. (2010) Studies in rheoencephalography (REG). J Electr Bioimp, 1:18–40. DOI: https://doi.org/10.5617/jeb.109
[31] Bodo M. (2020) A noninvasive, continuous brain monitoring method: rheoencephalography (REG) DRC Sustainable Future 1:94-110. https://doi.org/10.37281/DRCSF
[32] Szabo S, Totka Z, Nagy-Bozsoky J, Pinter I, Bagany M, Bodo M. Rheoencephalography: A non-invasive method for neuromonitoring. J Electr Bioimpedance. 2024 Mar 13;15(1):10-25. doi: 10.2478/joeb-2024-0003.
[33] Acharya J.N., Hani AJ, Cheek J, Thirumala P, Tsuchida T.N. (2016) American Clinical Neurophysiology Society Guideline 2: Guidelines for Standard Electrode Position Nomenclature. Neurodiagn J. 56:245-252. https://doi.org/10.1080/21646821.2016.1245558
[34] Baranyi L, Dannie M, Hooftalle K, Pearce FJ, Bodo M. DataLyser program. https://doi.org/10.13140/RG.2.2.21169.25442
[35] MATLAB Mathworks, Natick, MA. https://www.mathworks.com/products/new_products/latest_features.html
[36] Scholkmann F, Boss J, and Wolf M. (2012) An Efficient Algorithm for Automatic Peak Detection in Noisy Periodic and Quasi-Periodic Signals. Algorithms 5:588-603; https://doi.org/10.3390/a5040588
[37] Bishop S, Ercole A (2018) Multiscale Peak and Trough Detection Optimized for Periodic and Quasi-Periodic Neuroscience Data. Acta Neurochirurgia Suppl. 126:189-195. https://doi.org/10.1007/978-3-319-65798-1_39
[38] Fawcett T. An introduction to ROC analysis. Pattern Recognition Letters. 27 (2006) pp. 861-874. https://doi.org/10.1016/j.patrec.2005.10.010
[39] Bland J.M., Altman D.G. (1999) Measuring agreement in method comparison studies. Statistical Methods in Medical Research 1999; 8: 135 – 160
[40] de Moraes F.M., Rocha E, Barros F.C.D. (2022) Waveform Morphology as a Surrogate for ICP Monitoring: A Comparison Between an Invasive and a Noninvasive Method. Neurocrit Care. 37:219-227. https://doi.org/10.1007/s12028-022-01477-4
[41] Poupko B.Z, Reichman Y, Rappaport A, Ben-Ari S. (2013) Noninvasive intracranial monitor. US patent. US 2013/0109979 A1. US20070287899A1 - Non-Invasive Intracranial Monitor - Google Patents https://patents.google.com/patent/US20070287899A1/en
[42] Boraschi A, Spiegelberg A. et al (2023) The effect of body position change on noninvasively acquired intracranial pulse waves. Physiol Meas. 44(3). https://doi.org/10.1088/1361-6579/acc3d6

[43] Shtok V.N. (1971) Povysheie vnutricherepnogo davleniia i diagnosticheskie vozmozhnosti reoéntsefolografii [Increased intracranial pressure and the diagnostic possibilities of rheoencephalography]. Vopr Neirokhir. 35:21-4. Russian. PMID: 5570270

[44] Sokolov V.I. (1985) Sostoianie gemodinamiki i zheludochkovoĭ sistemy golovnogo mozga pri antiortostaticheskom vozdeĭstvii -15 gradusov [Hemodynamic and cerebral ventricular functions during head-down tilt at -15 degrees]. Kosm Biol Aviakosm Med. 19:39-42. Russian. PMID: 3990231

[45] Iarullin Kh. Kh, Gornago V.A, Vasil'eva T.D, Gugushvili M.E. (1980) Izuchenie prognosticheskoĭ znachimosti antiortostaticheskoĭ nagruzki [Prognostic importance of the head-down tilting load]. Kosm Biol Aviakosm Med. 14:48-54. Russian. PMID: 7382406

[46] Moskalenko Yu. E, Beketov A.I. et al (1991) The involvement of cerebrovascular reactivity in pathogenesis of space motion sickness. Acta Astronaut. 23:97-103. https://doi.org/10.1016/0094-5765(91)90104-d

[47] Matsnev E.I., Iakovleva I.I. et al (1990) Osobennosti techeniia bolezni dvizheniia pri dlitel'noĭ otolitovoĭ stimuliatsii v antiortostaticheskom polozhenii [Characteristics of motion sickness during prolonged otolith stimulation in anti-orthostatic position]. Vestn Otorinolaringol. 1:8-14. Russian. PMID: 2316129.

[48] Sheel A.W., Romer L.M. (2012) Ventilation and respiratory mechanics. Compr. Physiol. 2:1093-142. https://doi.org/10.1002/cphy.c100046

[49] Perez J.J. (2014) To what extent is the bipolar rheoencephalographic signal contaminated by scalp blood flow? A clinical study to quantify its extra and nonextracranial components. Biomed Eng Online. 13 -131;1-11 https://doi.org/10.1186/1475-925X-13-131

[50] Barrit S, E., Hadwe S, A., Barajraji M, Torcida N, Bogossian E.G, André J, Niset A, Carron R, Taccone F.S, Madsen J. Complications of Intracranial Multimodal Monitoring for Neurocritical Care: A Systematic Review and Meta-Analysis. Neurocrit Care. 2024 Jun;40(3):1182-1192. https://doi.org/10.1007/s12028-023-01885-0.

[51] Wei M, Krakauskaite S, Subramanian S, Scalzo F. Peak detection in intracranial pressure signal waveforms: a comparative study. Biomed Eng Online. 2024 Jun 24;23(1):61. https://doi.org/10.1186/s12938-024-01245-9. PMID: 38915091; PMCID: PMC11194974.

[52] Brady K.M., Mytar J.O., Kibler K.K. et al (2010) Monitoring cerebrovascular pressure reactivity with rheoencephalography. J. Phys.: Conf. Ser. 224 012089 https://doi.org/10.1088/1742-6596/224/1/012089

[53] Montgomery LD, Montgomery RW, Bodo M, Mahon RT, Pearce FJ. Thoracic, Peripheral, and Cerebral Volume, Circulatory and Pressure Responses to PEEP During Simulated Hemorrhage in a Pig Model: a Case Study. J Electr Bioimpedance. 2021 Dec 27;12(1):103-116. doi: 10.2478/joeb-2021-0013.

[54] Chang JJ, Gensler R, Armonda RA, Bodo M. Validation Studies on a Noninvasive Neuromonitoring Method, Rheoencephalography - A Review. Clinical Neuroscience - 2025;79 In print

[55] Claassen JAHR, Thijssen DHJ, Panerai RB, Faraci FM. Regulation of cerebral blood flow in humans: physiology and clinical implications of autoregulation. Physiol Rev. 2021 Oct 1;101(4):1487-1559. doi: 10.1152/physrev.00022.202.

[56] Barnes JN. Sex-specific factors regulating pressure and flow. Exp Physiol. 2017 Nov 1;102(11):1385-1392. doi: 10.1113/EP086531.

[57] Bögli SY, Beqiri E, et al. Unlocking the potential of high-resolution multimodality neuromonitoring for traumatic brain injury management: lessons and insights from cases, events, and patterns. Crit Care. 2025 Mar 31;29(1):139. doi: 10.1186/s13054-025-05360-4.

[58] NASA Technology Readiness Levels - NASA Earth Science and Technology Office https://esto.nasa.gov/trl/

[59] Bodo M, Thuroczy G, Nagy I, Peredi J, Sipos K, Harcos P, Nagy Z, Voros J, Zoltay L, Ozsvald L. A complex cerebrovascular screening system (CERBERUS). Med Prog Technol. 1995 May;21(2):53-66. PMID: 7565396.

[60] Bodo M, Pearce FJ, Tsai MCD, Garcia A, vanAlbert S, Armonda R. Cessation of vital signs monitored during lethal hemorrhage: a Swine study. J Spec Oper Med. 2013 Winter;13(4):63-75. doi: 10.55460/20NR-BE1R.

[61] Meghdadi AH, Popovic D, Rupp G, Smith S, Berka C, Verma A. Transcranial Impedance Changes during Sleep: A Rheoencephalography Study. IEEE J Transl Eng Health Med. 2019 Feb 11;7:2700107. doi: 10.1109/JTEHM.2019.2898193

[62] Kas'yan II, Vainshtein GB, Semernya VI, Gorokhov KA, Tikhonov VP, Ponomarev SI, Asanov KK. Pattern of blood circulation in the brain during rest and functional tests by Salyut-4 space crewmen. Biol Bull Acad Sci USSR. 1980 Mar-Apr;7(2):83-9. PMID: 7225468.

[63] Bodo M, Szebeni J, Baranyi L, Savay S, Pearce FJ, Alving CR, Bünger R. Cerebrovascular involvement in liposome-induced cardiopulmonary distress in pigs. J Liposome Res. 2005;15(1-2):3-14. doi: 10.1081/lpr-64523.